

Original Article

Cite this article: Neogi S, Bhardwaj A, and Kundu A (2022) Evolution of Neoproterozoic Shillong Basin, Meghalaya, NE India: implications of supercontinent break-up and amalgamation. *Geological Magazine* 159: 628–644. <https://doi.org/10.1017/S0016756821001230>

Received: 11 May 2021

Revised: 29 October 2021

Accepted: 30 October 2021

First published online: 9 December 2021

Keywords:

Shillong Basin; Meghalaya; Rodinia break-up; stratigraphy; structure; Pan-African Orogeny

Author for correspondence: Susobhan Neogi,
Email: susobhanneogi@gmail.com

Evolution of Neoproterozoic Shillong Basin, Meghalaya, NE India: implications of supercontinent break-up and amalgamation

Susobhan Neogi¹ , Apoorve Bhardwaj² and Amitava Kundu³

¹Geological Survey of India, 15A & B, Kyd Street, Kolkata 700016, India; ²Geological Survey of India, Lucknow, Uttar Pradesh 226024, India and ³Geological Survey of India, Chennai, Tamil Nadu 600032, India

Abstract

Fragmentation and amalgamation of supercontinents play an important role in shaping our planet. The break-up of such a widely studied supercontinent, Rodinia, has been well documented from several parts of India, especially the northwestern and eastern sector. Interestingly, being located very close to the Proterozoic tectonic margin, northeastern India is expected to have had a significant role in Neoproterozoic geodynamics, but this aspect has still not been thoroughly studied. We therefore investigate a poorly studied NE–SW-trending Shillong Basin of Meghalaya from NE India, which preserves the stratigraphic record and structural evolution spanning the Neoproterozoic Era. The low-grade metasedimentary rocks of Shillong Basin unconformably overlie the high-grade Archean–Proterozoic basement and comprise a c. 4000-m-thick platform sedimentary rock succession. In this study, we divide this succession into three formations: lower Tarso, middle Ingsaw and upper Umlapher. A NW–SE-aligned compression event later caused the thrusting of these sedimentary rocks over the basement with a tectonic contact in the western margin, resulting in NE–SW-trending fold belts. The rift-controlled Shillong Basin shows a comparable Neoproterozoic evolution with the equivalent basins of peninsular India and eastern Gondwana. The recorded Neoproterozoic rift tectonics are likely associated with Rodinia's break-up and continent dispersion, which finally ended with the oblique collision of India with Australia and the intrusion of Cambrian granitoids during the Pan-African Orogeny, contributing to the assembly of Gondwana. This contribution is the first to present a complete litho-structural evolution of the Shillong Basin in relation to regional and global geodynamic settings.

1. Introduction

The Neoproterozoic Era witnessed global continental reorganization, resulting in the two major supercontinental assemblies of Rodinia (Fig. 1a; through the Grenvillian Orogeny) and Gondwana (Fig. 1b; through the Pan-African Orogeny) (Collins & Pisarevsky, 2005; Li *et al.* 2008; Rino *et al.* 2008; Bradley, 2011; Cawood *et al.* 2013; Arora *et al.* 2020). Meso- to Neoproterozoic amalgamation of Rodinia took place between 1100 and 900 Ma (Kröner & Cordani, 2003; Li *et al.* 2008; Gregory *et al.* 2009; Cawood *et al.* 2013; Jing *et al.* 2020), and it eventually broke apart during 750–720 Ma (Fig. 1a) (Gregory *et al.* 2009; Jing *et al.* 2020). The Gondwana supercontinent merged following the break-up and dispersion of Rodinia's constituents between 750 and 530 Ma during the Pan-African Orogeny (Collins & Pisarevsky, 2005) (Fig. 1b). However, transitional phases of Rodinia break-up and Gondwana amalgamation in the rock record are scarce and can only be traced back to a limited extent from stable crustal deposits within Neoproterozoic basins.

In India, Archean cratons in the north (Aravalli and Bundelkhand) and south (Bastar, Singbhum and Dharwar) were accreted through Proterozoic mobile belts to form a stable continental mass that primarily represents the Proterozoic framework (Fig. 1c). The volcano-sedimentary association of the mobile belts surrounding the Archean nucleus (Central Indian Tectonic Zone, Assam Meghalaya Gneissic Complex, Chottanagpur Gneissic Complex and Eastern Ghats Mobile Belt) was episodically metamorphosed and deformed from 2500 to 1000 Ma, reaching complete stability during late Mesoproterozoic time (1000 Ma) during the Rodinia amalgamation (Bhowmik, 2019). The Mesoproterozoic and Neoproterozoic evolutionary histories of Indian tectonic belts are separated by intense tectonothermal activity at 1000 Ma (Chaudhuri *et al.* 1999). The opening up of rifted ocean basins along the periphery of Archean–Proterozoic stable crusts indicates a short spell of tectonic instability during early Neoproterozoic time (Fig. 1c) (Kale & Phansalkar, 1991; Chaudhuri *et al.* 1999; Chakraborty *et al.* 2020).

The Neoproterozoic basins of India are represented by the Rewa and Bhandar Group of the upper Vindhyan Basin, the Kurnool Group of the Cuddapah Basin, the Sullavai Group of the

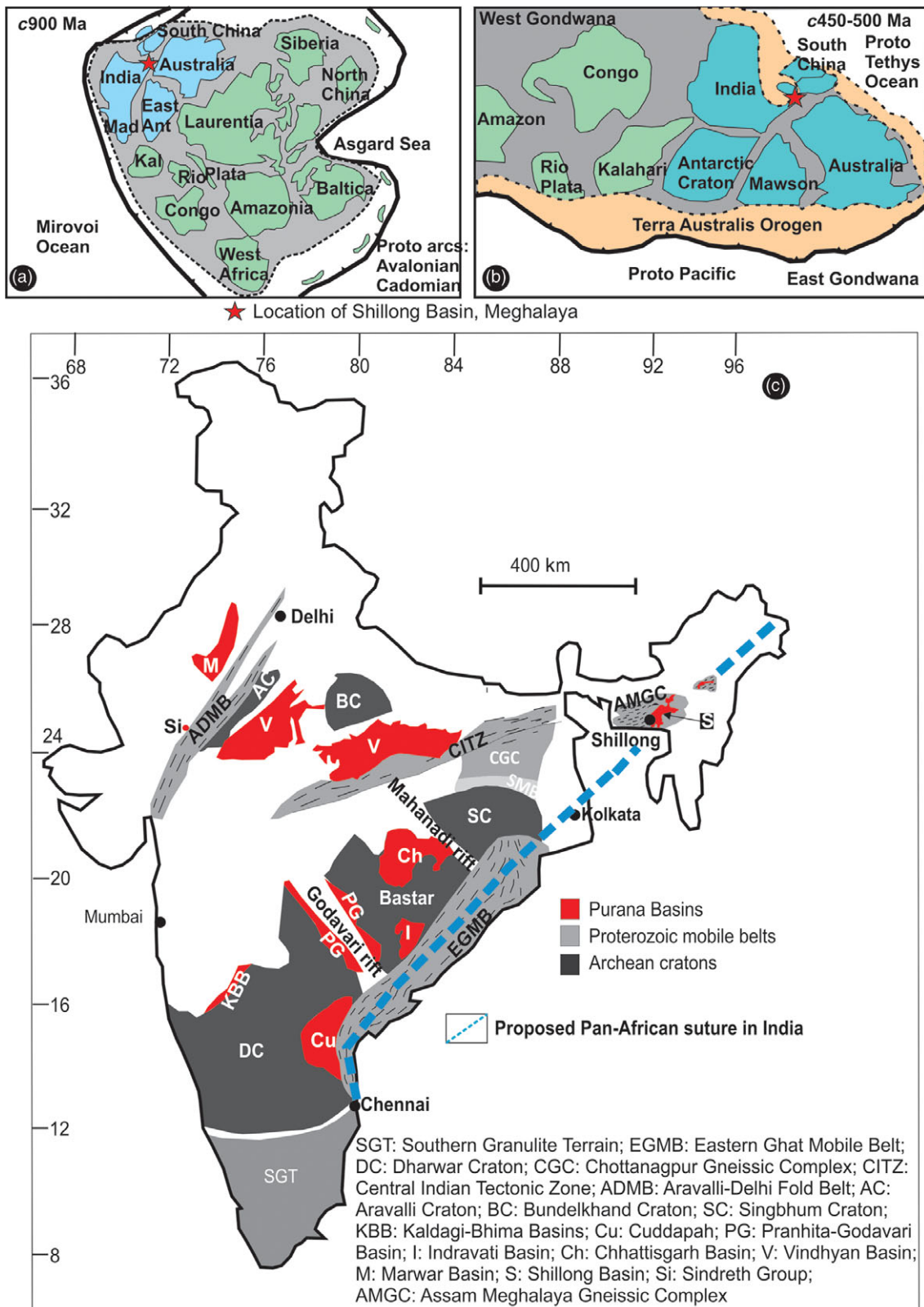


Fig. 1. (Colour online) (a) Position of India and Shillong Basin in Rodinia (modified after Cawood *et al.* 2013) and (b) Gondwana configuration (modified after Cawood *et al.* 2013). (c) Proterozoic map of India highlighting the distribution of major Archean cratons, Proterozoic mobile belts and Neoproterozoic basins (modified after Mishra, 2015). The blue dotted line in the eastern part is the proposed Pan-African suture from the EGMB to the Shillong Basin in the NE.

Pranhita–Godavari Basin, the Marwar Supergroup and the Sindreth Group of western India, Bhima Group of Bhima Basin and the Badami Group of the Kaladgi basin (Fig. 1c) (Chaudhuri *et al.* 1999; Nagarajan *et al.* 2011; George & Ray, 2017; Schöbel *et al.* 2017; Joy *et al.* 2019). The Neoproterozoic basins of India feature a common evolution pattern in which the basins first opened up with rifting and subsequently evolved into a stable platformal condition. (Chaudhuri *et al.* 1999). The consistent base of the Neoproterozoic basins of peninsular and extra-peninsular India is represented by a typical conglomerate and/or tuff of fan delta deposits, while basin fill sediments show a fining-upwards sequence associated with a major transgression (Chaudhuri *et al.* 1999; Joy *et al.* 2019). The lower sections of all the Neoproterozoic basins show traces of tectonic upheaval, but the upper sections retain rather stable shallow-water deposits (Chaudhuri *et al.* 1999).

The evolution of Neoproterozoic basins in India is comparable to that of other east Gondwana basins (the Officer Basin, Savory Basin, Adelaide Basin of Australia, Nanhua Basin of South China and Beardmore Group of East Antarctica), where all basins are riftogenic in origin and linked to Rodinia break-up (Walter *et al.* 1995; Chaudhuri *et al.* 1999; Goodge *et al.* 2002; Zhou *et al.* 2009; Bose *et al.* 2020; Kumar *et al.* 2020; Lloyd *et al.* 2020).

We focus on the tectonic evolution of the Shillong Basin of Meghalaya, which represents an isolated Proterozoic basin in NE India (Fig. 2b). It unconformably overlies the high-grade basement (i.e. Assam Meghalaya Gneissic Complex). According to a number of publications, the Shillong Basin is very close to the tectonic margins of the Rodinia and Gondwana supercontinents (Collins & Pisarevsky, 2005; Cawood *et al.* 2013; Pant & Dasgupta, 2017; Arora *et al.* 2020), and could therefore be a key link in reconstructing Proterozoic geodynamic processes. However, little is known about the evolutionary history of the Shillong Basin. We therefore evaluate the evolution of the Shillong Basin by detailed mapping (220 km²), deformation fabric analysis, petrography, geochemistry and the incorporation of existing geochronological data, as well as considering its possible link to the Rodinia and Gondwana supercontinents. Accordingly, we focused on the west-central section of the Shillong Basin, which preserves the entire litho package, as well as diastrophic and non-diastrophic structures that assisted in its evolution.

2. Geological settings

The Assam Meghalaya Gneissic Complex (AMGC) is an isolated, tectonically detached Archean–Proterozoic block located in the northeastern part of India in Meghalaya (Fig. 2a, b). It has been described as an uplifted horst-like feature that is bordered in the south by the E–W-aligned Dauki Fault and in the north by the Brahmaputra Fault (Bilham & England, 2001; Nandy, 2001) (Fig. 2b). Younger low-grade metasediments overlie the older AMGC and constitute the Proterozoic mosaic of the Meghalaya (Yin *et al.* 2010) (Fig. 2b). Meta-mafic rocks (Ray *et al.* 2013) and Cambrian granitoids (Kumar *et al.* 2017) intrude the former sequence. The Cretaceous Sylhet Trap, ultramafic–alkaline–carbonate complex and Cretaceous–Tertiary sedimentary rocks cover the southern part of the plateau (Nandy, 2001).

The Neoproterozoic–Mesoproterozoic high-grade basement rocks of AMGC is represented by para- and ortho-gneisses (Lal *et al.* 1978; Bidyananda & Deomurari, 2007; Chatterjee *et al.* 2007; Chatterjee *et al.* 2015; Kumar *et al.* 2017; Neogi *et al.* 2017).

These basement gneisses exhibit at least three stages of deformation and related metamorphisms (Lal *et al.* 1978; Ray *et al.* 2011, 2013; Neogi & Pal, 2021). D₁ imprints are rarely preserved and are transposed by D₂ deformation, with E–W-aligned chains of D₂ antiforms and synforms dominating the map pattern (Lal *et al.* 1978; Chatterjee *et al.* 2007; Neogi & Pal, 2021). Different areas of the AMGC have shown peak metamorphism at around 750°C and 5–6 kbar (Lal *et al.* 1978; Neogi *et al.* 2017). Monazites (U–Th–Pb age) associated with AMGC metasediments revealed three stages of thermal growth at: 1600–1400, 1200–1000 and 500–450 Ma (Chatterjee *et al.* 2007; Neogi *et al.* 2017; Borah *et al.* 2019).

The deformed, NE–SW-oriented Shillong Basin is exposed in the east-central Meghalaya Plateau, unconformably overlying the AMGC (Nandy, 2001) (Fig. 2b). The Tyrsad–Barapani Shear Zone marks the western boundary of the AMGC, Cretaceous–Tertiary sedimentary rocks cover the southern portion, the Shillong Basin has an unconformable contact with the basement (AMGC) in the east, and the northern contact lies below the Brahmaputra Quaternary (Fig. 2b) (Nandy, 2001). The Shillong Basin was mapped for the first time by Oldham (1858). The low-grade metasedimentary strata and associated volcanic rocks were named “Shillong Series” by Medicott (1869), which was later termed the Shillong Group by Mazumdar (1976). It has been further classified under two-fold (Barooah & Goswami, 1972; Ahmed, 1981; Bhattacharjee & Rahman, 1985; Anonymous, 2009; Sarma, 2014) and three-fold schemes (Khonglah *et al.* 2008). The Shillong Group metasedimentary rocks show polyphase deformation with a dominant NE–SW-aligned fabric (Murthy *et al.* 1976; Mitra, 1998; Khonglah *et al.* 2008) and greenschist facies metamorphism (Mitra, 1998; Devi & Sarma, 2010; Sarma, 2014). Many models have been proposed to characterize the Shillong Basin, including: (1) a linear Mio-geosynclinal basin (Mazumdar, 1986); (2) a sag basin (Nandy, 2001); (3) an extensional basin (Kakati & Sarma, 2013); and (4) a transtensional or pull-apart basin (Sarma, 2014).

3. Methodology

3.a. Structural mapping

A total of 220 km² of geological mapping has been completed by taking suitable geological traverses along and across the strike in the west-central part of the Shillong Basin, located in the NE Indian states of Assam and Meghalaya. The structural mapping was performed in the field by measuring the deformation fabrics. Fresh-surface and open-pit samples were collected from each litho-unit discussed.

3.b. Analytical technique

The selected samples were analysed for major and trace elements at the Geological Survey of India, Shillong, using a sequential wavelength dispersive X-ray fluorescence (WDXRF; Bruker S8 Tiger) equipped with a Rh tube. Fresh, unaltered samples were collected and chipped using a jaw crusher, cleaned with an ultrasonic vibrator, dried and powdered in a vibratory disc mill. The rock samples were crushed and pulverized to pass through a –200 micron mesh, then coned and quartered to ensure homogeneous mixing. The fusion beads and pressed pellets were then prepared for analysis. The pressed pellets were made from 4.5 g of finely ground sample (–200 mesh) and 1.13 g of cellulose binder. Because there is no calibration programme available for samples with such a matrix,

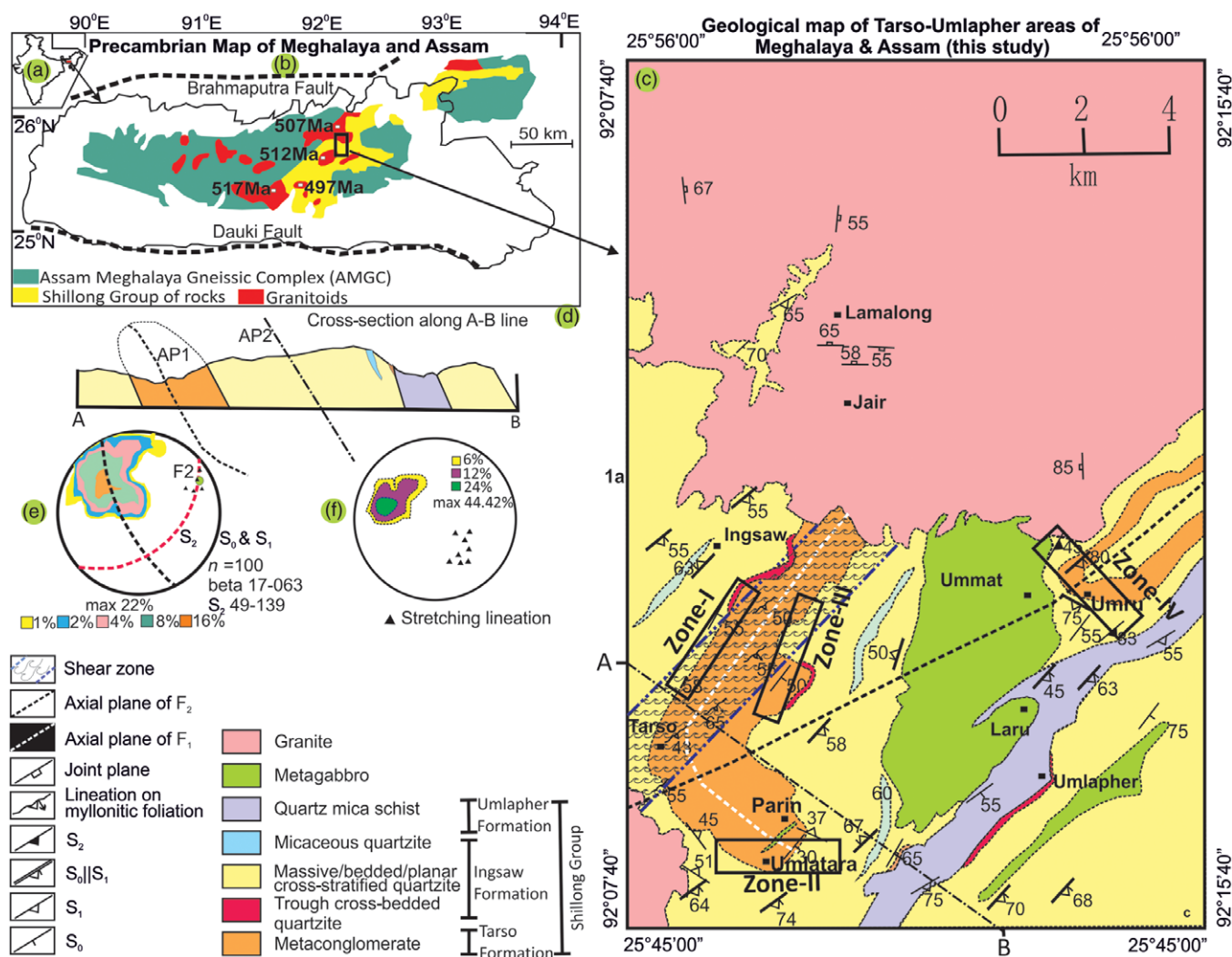


Fig. 2. (Colour online) (a) Location of Meghalaya within India; (b) simplified Precambrian geology of Meghalaya, with published (Kumar *et al.* 2017) Neoproterozoic geological constraints from the intruding granites to the Shillong Basin superimposed; (c) geological and structural map of Tarso-Umlapher areas (this study); (d) the first and second axial planes of the folds, AP1 and AP2, along the geological cross-section A–B, showing the assumed structural disposition of the beds at depth; (e) stereographic projection of the poles of beddings (S_0) and early foliations (S_1) showing the nature of regional fold (F_2); triangular marks are the measured F_2 axis; and (f) stereographic projection of the mylonitic foliations and stretching lineations measured from the Tarso Transpression Zone.

the data were generated from pressed pellets using the standardless software Quant express. The generated results were then analysed and corrected using loss on ignition (LOI) and dilution factors. Certified international standards were used during the analysis. The precision for SiO_2 and Al_2O_3 is 2 wt%, and 0.3 wt% for the other major oxides and trace elements. Table 1 summarizes the representative geochemical data for each of the nine samples.

4. Results

4.a. Geological mapping

4.a.1. Lithology

The field area exposes various Shillong Group units and intrusive gabbro and granitoids (Fig. 2c). The Shillong Group metasedimentary rocks are made up of a basal metaconglomerate, a middle quartzite and a quartz mica schist at the top (Fig. 2c). The meta-gabbros are intrusive to the sedimentary units, which are then intruded by granite. As the relative disposition of the

Shillong Group of metasedimentary rocks is modified by deformation, we will discuss the geographical and temporal heterogeneity of the lithounits in relation to their position in regional folds (online Supplementary Table S1, available at <http://journals.cambridge.org/geo>).

The bottom-most unit of the Shillong Group in the study area is a meta-conglomerate, which is exposed within the core of an anti-form (Fig. 2c). When unfolded, the thickness of the conglomerate is 400–500 m. Along and across its strike, the conglomerate showed considerable compositional change (in terms of clast and matrix). The mapped region has therefore been classified into four domains to explain the variety of clasts and matrixes (Fig. 2c).

Zone I. Near Tarso (Fig. 2c, Zone I), it consists of a fine-grained siliceous matrix with granite and vein quartz clasts (Fig. 3a). Clasts are poorly sorted, where extreme shearing has changed the initial roundness and sphericity. Clasts size varies from 1 mm to > 20 cm. Alternate clasts-rich and clasts-poor zones define the bedding, which is also gradational (Fig. 3a). However, the stratigraphic top could not be deciphered from the gradation due to

Table 1. Bulk-rock chemistry (major oxides and trace elements) of different units of Shillong Group.

Rock type Sample no.	Metaconglomerate (matrix)			Quartz mica schist				Quartzite	
	16	16a	18	25	30	25a	30a	24	24a
SiO ₂ (%)	73.61	73.81	65.41	77.41	77.13	77.72	77.65	77.85	78.25
TiO ₂ (%)	0.17	0.17	0.86	0.70	0.32	0.64	0.30	0.52	0.48
Al ₂ O ₃ (%)	13.52	13.57	16.37	11.85	11.78	11.70	11.48	12.29	12.01
Fe ₂ O ₃ (T) (%)	2.53	2.46	8.35	2.89	4.88	2.82	4.89	3.10	3.09
MnO (%)	0.04	0.04	0.07	0.02	0.02	0.02	0.02	0.04	0.03
MgO (%)	0.48	0.42	2.35	1.21	0.37	1.18	0.37	0.74	0.72
CaO (%)	0.01	0.01	< 0.01	< 0.01	< 0.01	< 0.01	< 0.01	0.01	0.01
Na ₂ O (%)	4.21	4.11	0.40	0.17	0.16	0.16	0.17	0.22	0.21
K ₂ O (%)	4.95	4.87	4.84	4.16	3.90	4.19	3.78	4.15	4.17
P ₂ O ₅ (%)	0.03	0.02	0.07	0.06	0.12	0.05	0.11	0.05	0.04
LOI (%)	0.16	0.20	1.01	1.36	1.05	1.31	0.94	0.77	0.74
Ba (ppm)	17	–	29	–	–	251	13	–	45
Co (ppm)	15	–	28	–	–	287	12	–	60
Cr (ppm)	19	–	25	–	–	382	5	–	73
Cu (ppm)	11	–	47	–	–	408	6	–	51
Ga (ppm)	15	–	12	–	–	129	< 3.5	–	< 2
Nb (ppm)	< 5	–	13	–	–	216	18	–	17
Ni (ppm)	< 5	–	5	–	–	15	57	–	< 2
Pb (ppm)	10	–	15	–	–	133	5	–	9
Rb (ppm)	16	–	14	–	–	158	8	–	18
Sc (ppm)	10	–	11	–	–	115	4	–	17
Sr (ppm)	17	–	29	–	–	251	13	–	45
Th (ppm)	15	–	28	–	–	287	12	–	60
V (ppm)	19	–	25	–	–	382	5	–	73
Y (ppm)	11	–	47	–	–	408	6	–	51
Zn (ppm)	15	–	12	–	–	129	< 3.5	–	< 2
Zr (ppm)	< 5	–	13	–	–	216	18	–	17

deformation. The individual bed thickness ranges from a few centimetres to more than 5 m (online Supplementary Table S1). The conglomerate at the east of Tarso is more of a gritty quartzite and grades laterally into pebbly horizons.

Zone II. Zone II (Fig. 2c) conglomerate has a siliceous and ferruginous matrix (Fig. 3b, d), and the clasts are poorly sorted (Fig. 3b, d). Clasts are mostly vein quartz with varying shapes (e.g. tabular, triangular and rhombic), roundness (e.g. angular, sub-angular and sub-rounded) and low sphericity (online Supplementary Table S1). Angular vein quartz clasts are dominant (Fig. 3d) and graded locally.

Zone III. Zone III conglomerate (Fig. 2c) is polymictic, with clasts of vein quartz, biotite gneiss and granite gneiss in an argillaceous matrix (Fig. 3f, i). The proportion of gneiss clasts to vein quartz clasts is c. 2–3%. Clasts with varying degrees of angularity are poorly sorted and range in size from 5 mm to 7 cm (online Supplementary Table S1). The matrix is highly foliated in this section, with muscovite and biotite defining the foliation.

Zone IV. The diversity of clasts composition increases in Zone IV (Fig. 2c) compared with other areas. Large gneiss boulders (> 50 cm) are found within the micaceous matrix (Fig. 3c, e). The relative abundance of gneiss clasts is greater than 5% in Zone IV, including quartz mica schist, biotite gneiss and vein quartz. The angular to sub-rounded poorly sorted clasts range in size from 5 mm to 1 m (online Supplementary Table S1).

Large (2–5 cm), idioblastic garnet and staurolite (Fig. 3j) growth is observed within the micaceous conglomerate at the margins of basic intrusives (Fig. 2c, Zone II and III).

Quartzite overlies the meta-conglomerate, forming NE–SW-aligned steep long ridges. Because of the low outcrop density, the proper litho contact between conglomerate and quartzite was not observed, but a gradational contact is inferred from the discrete outcrops. The quartzite has well-developed facies variation. The lowermost quartzite (2–5 m thick) is cross-bedded with thick bedding (10–30 cm) (Fig. 3k). However, the orientation of the original troughs has been too heavily modified by complex folding to infer the palaeo-flow direction. The lower quartzite is hard,



Fig. 3. (Colour online) Field photographs showing (a) massive, graded bedding in basal conglomerate; (b) conglomerate with clasts of vein quartz and granite set in a siliceous matrix; (c) boulder of biotite gneiss within conglomerate; (d) very poorly sorted vein quartz clasts floats in a siliceous and ferruginous matrix; (e) large rounded boulder of quartz mica schist within the argillitic matrix of basal conglomerate near Ummat; (f) clasts of various compositions and shapes scattered within the phyllitic matrix of conglomerate near Ummat; (g) extremely sheared and stretched pebbles of the conglomerate with very fine matrix near Tarso; (h) down-plunging stretching lineations over the steeply dipping mylonitic foliation in conglomerate near Tarso; (i) poorly sorted argillitic matrix-bearing conglomerate; clast size reduces dramatically with crenulated foliations; (j) random, idioblastic staurolite growth over the argillitic matrix of the conglomerate in contact with metagabbro intrusives near Ummat; (k) trough cross-stratified quartzite at contact with basal conglomerate near Ingsaw; (l) herringbone cross-stratified quartzite at the east of Ingsaw; (m) planar cross-stratified quartzite with reverse younging direction; (n) thick pile of quartzite and micaceous quartzite intercalation; (o) outcrop of magnetite-bearing quartz mica schist; (p) exposure of metagabbro; and (q) outcrop of Kyrdem Granite with xenoliths of quartzite from Ingsaw Formation.

bouldery, and has rounded cavities and iron staining in most cases. The upper herringbone cross-stratified quartzite is in gradational contact with the trough cross-bedded quartzite (Fig. 3l). Due to extreme weathering, the herringbone structure is only found in outcrops of 1–2 m width in this study. The mid-erosional surface between the foresets of the herringbone cross-beds has been preserved irregularly (Fig. 3l).

The middle quartzite is dominated by planar and tabular cross-beds that overlie the lower quartzite (Fig. 3m) but are mostly in direct contact with the meta-conglomerate (Fig. 2c). It is intercalated with micaceous quartzite (Fig. 3n) and, on rare occasions, with thin carbonaceous phyllite. However, it appears massive and friable, with irregular bedding in many outcrops. Numerous overturned planar cross-beddings are identified, indicating a stratigraphic inversion caused by deformation (Fig. 3m).

In comparison to the middle quartzite, the uppermost quartzite is trough cross-bedded and relatively hard. On occasion, ripple drift cross-laminations were observed. Ripple marks or casts are observed in nearby areas but not recorded in the mapped area. These have a low-amplitude and a moderate wavelength, as well as a nearly straight crest line and rounded troughs.

Magnetite-bearing quartz mica schist is the uppermost unit of the Shillong Group. It is greyish, hard and forms a prominent NE–SW-aligned ridge in the central part of the mapped area (near Umlapher) (Fig. 2c). The rock is made up of 25% quartz, 50% mica, 20% feldspar and 5% magnetite. Magnetite grains are scattered throughout the unit (Fig. 3o), and it is finely laminated. Muscovite defines the foliation and runs parallel to the bedding.

Metagabbro occurs as NE–SW-aligned linear intrusives in the lower elevated parts of the study area (near Ummat, Laru) that run sub-parallel to the axial plane of the regional folds (F₂) (Fig. 2c). It is very coarse near the centre of the pluton and relatively fine towards the margin, and it is composed of amphibole (40–45%), plagioclase (50–55%) and magnetite (1–2%). It retains a relic interlocking texture with undeformed grain boundaries (Fig. 3p). However, at the edge of the plutons, it is crudely foliated.

Granite is found in two intrusive plutons in the northern and southern parts of the study area. The Kyrdem Granite is to the SW, and a portion of the Nongpoh Granite is to the north (Fig. 2c). The Kyrdem Granite is coarse, pink, porphyritic and composed of quartz (50%), K-feldspar (30%), plagioclase (15%), biotite (5%), pyrite and magnetite (Fig. 3q). Plagioclase dominates over K-feldspar. The phenocrysts are of K-feldspar (2 mm to 7 cm in size) and plagioclase, while the groundmass is of quartz, K-feldspar, plagioclase, biotite, pyrite and magnetite. Mafic microgranular enclaves (MME) of various shapes and sizes, as well as xenoliths of Shillong Group rocks (Fig. 3q), are common.

The Nongpoh Granite is fine-grained and non-porphyritic near the edge of the pluton, but coarse-grained and porphyritic in the centre. Quartz, K-feldspar, plagioclase, biotite and magnetite contribute to the groundmass, whereas phenocrysts are euhedral K-feldspar and plagioclase. The size of the MMEs is unlike those found in the Kyrdem Granite and is relatively smaller.

4.a.2. Structure

The repetition of the lithounits demonstrates deformation in the metasedimentary rocks (Fig. 2c, d). Rocks are doubly folded in areas where bedding (S₀) became sub-parallel to early foliation (S₁). The dominant fabric of the study area is bedding (S₀) with early foliation (S₁), and the foliation is also axial planar to the rarely preserved first folds (F₁). The microlithon and cleavage domains of S₁ consist of quartz (or feldspar) and micaceous layers

(muscovite with little biotite), respectively. Because the prominence of S₁ is dependent on the availability of mica within the rocks, S₁ is rarely developed in quartzite. The overall bedding and foliation (S₁) trend of the rocks is NE–SW with a moderate to low southerly dip (except in the hinges).

F₁ folds are rootless and tight with low interlimb angles. Broadly rounded hinges, a high amplitude and short wavelength are the characteristics of these folds. The geometry of the F₁ folds varies from reclined to recumbent to upright on different parts of the late fold (F₂) profile. However, due to a lack of data, the F₁ plunge and pole of axial planes are not considered for statistical analysis.

F₂ is represented by the regional chain of overturned antiforms and synforms. Mesoscopic, congruous F₂ folds are close, upright, moderately NE-plunging with SE-dipping axial plane. F₂ folds within the micaceous units are crenulated, whereas quartzite display outcrop-scale folds. Characteristically, F₂ folds are flexural slip folds with interlayer slips and tension gashes. The statistically defined fold axis (β) of F₂ plunges 17° towards 63° and the dip of the axial plane is 49° towards 138° (Fig. 2e). Axial planar S₂ (defined by the alignment of muscovite) is weakly developed within the micaceous units as a crenulation cleavage. It is sub-parallel to S₀ and S₁ near the limb of F₂, and at a high angle at the hinge.

The closure near Umlatara (SW part) represents the closure of a first-generation fold (F₁), whereas the closure near Umru is a congruous higher-order F₂ fold (Fig. 2c). F₁ and F₂ plunge in the same direction; however, the F₁ axial plane is folded, and F₂ axial surface is flat (Fig. 2c). Superposition of F₂ over F₁ is coaxial, and a hook-shaped morphology has resulted from it. Moreover, the mapped area displays a NE–SW-aligned F₂ antiform, where the F₁ antiform lies on the western limb of the F₂. The overall southeastern dip of S₀ or S₁ indicates the overturned nature of F₂. Stratigraphic inversion is further supportive of overturned F₂ (Fig. 3m).

S₃ is the last regional deformation within the Shillong Group sedimentary rocks, and is a broad warp on map scale. The wide-spaced axial planar fracture is NNW–SSE-aligned and steeply dipping towards the ESE.

A NE–SW-aligned, wide, crustal-scale transpression superimposed on the early deformation fabrics is reported from the southern part of the study area (Fig. 2c). Throughout the zone, extreme grain size refinement, significant mylonitic foliation and well-defined downdip stretching lineations have been seen (Fig. 3g, h). The map width of the shear zone varies from 1 to 1.5 km with a maximum thickness reported near Tarso. The shear zone is mostly confined within the metaconglomerate and further extends along the NE, where it cuts the bottom quartzite (Fig. 2c). In metaconglomerate, the maximum instantaneous stretching axes of the deformed clasts lie in the downdip direction (Fig. 3h). The trend of the mylonitic foliation varies from 25 to 60° E and dips moderately (40–55°) towards the SE. Stretching lineations plunge moderately (50–55°) to the SE (Fig. 2f) and create an angle of > 80° with the deformation zone boundary measured on a plane parallel to the foliation and parallel to the lineation. On a plan view, tension gashes show both sinistral and dextral asymmetries. Few of the quartz veins are intruded parallel to the mylonite foliation. Moreover, a horizontal movement with a vertical stretching lineation is characteristics of the Tarso transpression zone.

4.b. Petrography

A total of 30 representative thin-sections from different lithounits were studied to understand their mineralogy and texture.

4.b.1. Meta-conglomerate

The siliceous matrix-bearing metaconglomerate is medium grained, and poorly sorted with quartz (70–75%), feldspar (10–15%) and secondary muscovite (alteration product of K-feldspar) (10–20%) as major mineral phases (Fig. 4d). Clasts of vein quartz within the matrix exhibit undulose extinction. Occasional large, fresh K-feldspar (Fig. 4e) and plagioclase (Fig. 4f) are preserved. The crude/strong external foliation of the matrix (S_1) is defined by muscovite and/or rare biotite that abut against the internal foliation of the clasts (Fig. 4d). Graded bedding often remains on a micro-scale within the matrix.

In the micaceous matrix, the relative proportion of muscovite (and biotite) is much higher (> 50%) than the abovedescribed type. The rock is poorly sorted with a varying degree of angularity and roundness (Fig. 4h). Muscovite and biotite define a developed, well-defined foliation within the matrix, and in many occasions the foliation is crenulated (Fig. 4h). Most of the idioblastic muscovites are secondary. The growth of magnetite, staurolite and garnet superimposed the early foliations (S_1) and postdate it (Fig. 4i, j).

Clasts of vein quartz and quartz-feldspar rock are prevalent near Tarso and surrounding regions (Zone I) (Fig. 4d). These clasts are poorly sorted with size ranging from < 1 mm to > 15 cm. However, original shapes of the clasts are modified by the shear deformation. Clasts of Zone I are of various shapes, sizes and most are of vein quartz. In Zone III, clasts are highly angular, randomly oriented and are mainly of vein quartz with occasional quartz-muscovite schist (Fig. 4g). In Zone IV, clasts are mainly of vein quartz, quartz biotite schist, quartz muscovite schist and granite gneiss (Fig. 4a–c).

4.b.2. Quartzite

The quartzite is medium- to coarse-grained, angular- to sub-rounded with siliceous cement (Fig. 4k). Quartz (80–85%) and feldspar (10–15%) are the major constituents with minor muscovite (< 5%). Secondary overgrowth, recrystallization and granulation of quartz along the margins are commonly observed. Grain boundaries are sutured with deformed and undulose extinctions. Feldspars are mostly decomposed and altered to clay minerals and muscovite (Fig. 4k). The lower part of the quartzite is dominantly arkosic (> 25% feldspar), but the middle and the top parts are micaceous. Magnetite and rutile are accessory phases. In the more micaceous quartzite, micas are aligned to define the S_1 foliation.

4.b.3. Magnetite-bearing quartz mica schist

This is a medium-grained, foliated rock, composed of quartz, feldspar, muscovite, biotite and magnetite (Fig. 4l). Quartz represents c. 25% of the total composition and feldspars are mostly altered to muscovite. The quartz grains are triangular-shaped, crescent-shaped and sub-angular (Fig. 4l), deformed with undulose extinction and very poorly sorted. Muscovite defines a strong foliation (S_1) while euhedral magnetites are randomly scattered.

4.c. Geochemistry

The SiO_2 content of the representative conglomerate matrix ranges from 65.41 to 73.61 wt%, while the Al_2O_3 value varies from 13.52 to 16.37 wt% (Table 1). FeO has a wide range of concentration varying from 2.53 to 8.53 wt%. MgO and Na_2O exhibit significant variation, ranging from 0.48 to 2.35 wt% and 0.4 to 4.21 wt% respectively. K_2O has little variation and is c. 4.8 wt%.

Quartzite is composed of 78 wt% SiO_2 , 12 wt% Al_2O_3 , and minor amounts of FeO (3%) and K_2O (4%). (Table 1).

The quartz mica schist is chemically uniform, with SiO_2 (78 wt%) and Al_2O_3 (12 wt%) accounting for 90% of the bulk composition (Table 1). Apart from that, a minor amount of FeO (2.82–4.88 wt%), MgO (0.37–1.21 wt%) and K_2O (3.90–4.19 wt%) contribute to the overall composition.

4.d. Metamorphism

The preservation of primary sedimentary structures within the Shillong Group metasedimentary rocks suggests that limited recrystallization occurred during thermal metamorphism. The Shillong Group's peak metamorphic mineral assemblages (chlorite, muscovite and/or biotite) indicate a lower greenschist facies. Because these rocks lack metamorphic index minerals, estimating the precise peak metamorphic condition using published ion-exchange thermo-barometers is difficult. Similarly, the preservation of primary igneous texture in metagabbro does not support a prograde metamorphism event; rather, these are metasomatized or altered during regional tectono-thermal events.

Localized garnet and staurolite growth are purely post-tectonic to regional foliation (S_1) (Fig. 4i, j) and are the result of contact metamorphism during basic rock emplacement. This interpretation is supported by the limited appearance of garnet and staurolite at the intrusive contact.

5. Discussion

5.a. Stratigraphy of the Shillong Group

The Shillong Group stratigraphy is debatable. The main constraints to describing the Shillong Basin stratigraphy are a lack of exposure continuity, marker horizons and compiled geological maps. The polyphase deformation of the units complicates the description and interpretation of the entire litho package. Many attempts were made to classify the Shillong Group (Medlicott, 1869; Barooah & Goswami, 1972; Ahmed, 1981; Bhattacharjee & Rahman, 1985; Khonglah *et al.* 2008; Devi & Sarma, 2010). Khonglah *et al.* (2008) and Devi & Sarma (2010) proposed threefold and twofold classifications, respectively (see online Supplementary Fig. S1). The Shillong Group was subdivided into a Lower Metapelitic Formation (LMF) and an Upper Quartzitic Formation (UQF) in the twofold classification scheme (see online Supplementary Fig. S1). The threefold classification of Khonglah *et al.* (2008) subdivides the group into a lower Mawlyndep Formation, middle Umium Formation and upper Nongpiur Formation. The Mawlyndep Formation is defined by basal polymictic conglomerate followed by quartzite. The Umium Formation is dominated by phyllite, black shale, meta-acid volcanic rocks and tuff. The Nongpiur Formation starts with a basal polymictic conglomerate accompanied by quartzite (see online Supplementary Fig. S1).

According to Devi & Sarma (2010), the Shillong Group was deposited unconformably over basement gneisses (AMGC). On the other hand, Khonglah *et al.* (2008) argued for the presence of the Umsning Schist Belt (USB) between the AMGC and the Shillong Group (see online Supplementary Fig. S1) and reported that the USB was the Shillong Group's oldest member. Neither the twofold nor the threefold classification is represented on any regional map of Meghalaya or the Shillong Basin (Fig. 2b). Both schemes also fail to explain the regional distribution of the Shillong Basin in a deformed terrain.

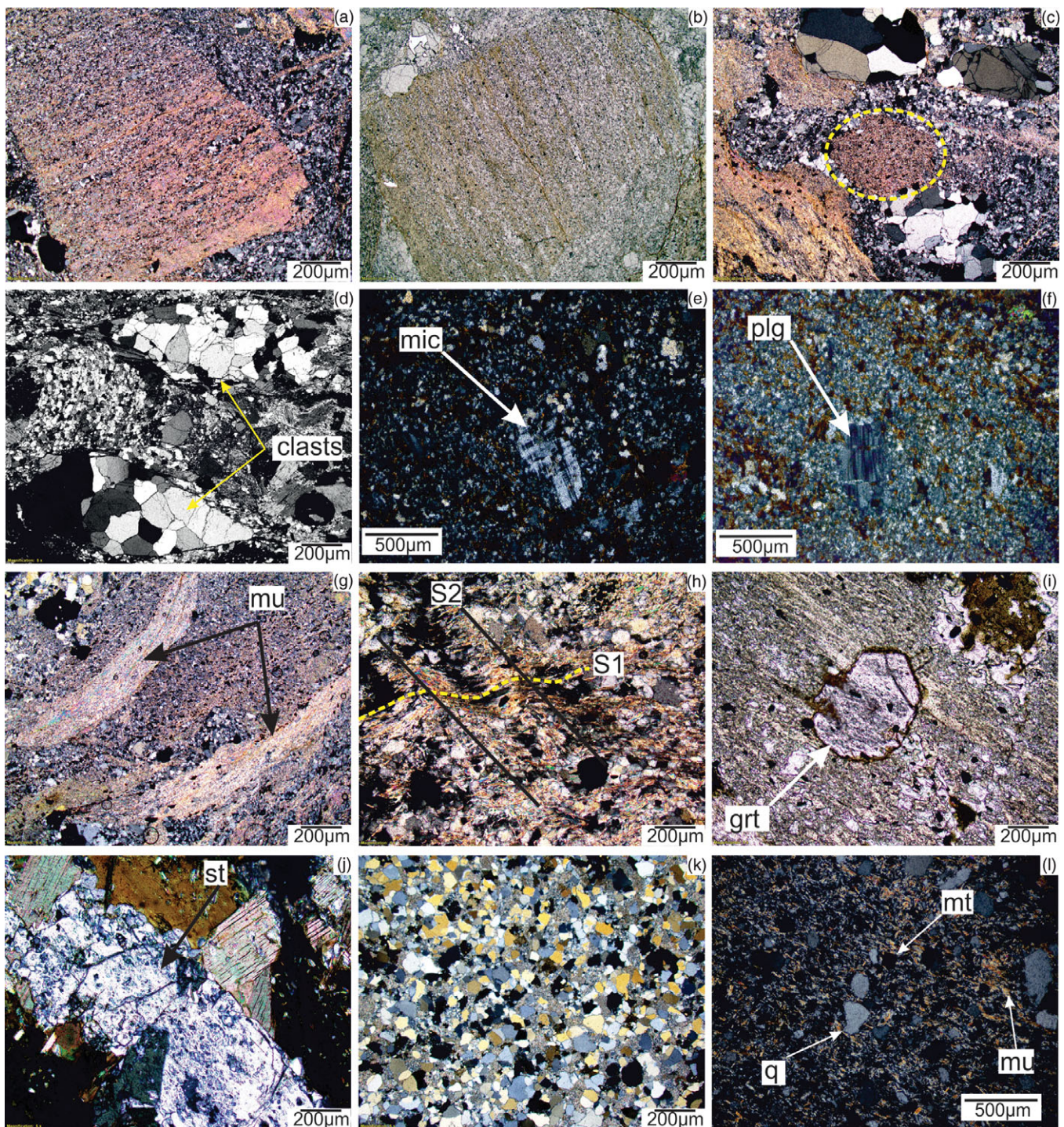


Fig. 4. (Colour online) Photomicrographs showing (a) rectangular clast of quartz mica schist within siliceous matrix of conglomerate; (b) clast of quartz biotite schist within micaceous matrix of conglomerate; (c) clasts of vein quartz and feldspathic material, now converted to secondary muscovite in conglomerate; (d) oval-shaped vein quartz clasts with siliceous matrix in conglomerate; (e) fresh crystal of microcline within the siliceous matrix of conglomerate; (f) unaltered, the euhedral crystal of plagioclase within a siliceous matrix of conglomerate; (g) elongated clasts, now altered to secondary muscovite within phyllitic matrix of the conglomerate; (h) the early foliation (S_1) of the phyllitic matrix of conglomerate is crenulated, axial planar foliation of those crenulations are S_2 ; (i) post-tectonic garnet, superimposed over the early foliation of the phyllitic matrix of conglomerate; (j) large post-tectonic staurolite within the phyllitic matrix of conglomerate; (k) overall texture and mineralogy of quartzite; feldspar within the intergranular spaces of quartz is altered to secondary muscovite; and (l) overall mineralogy and texture of the magnetite-bearing quartz mica schist. The shape of the quartz grains is crescent, triangular and elliptical. Mineral abbreviations after Kretz (1983).

In the present study, the Shillong Group litho-package is represented by a thick matrix-supported polymictic metaconglomerate at the base, followed by quartzite–micaceous quartzite interlayers and magnetite-bearing quartz mica schist at the top

(see online Supplementary Fig. S1). The basement, however, is not exposed in the mapped area, but is recorded from further east where the metaconglomerate lies just above the biotite gneiss basement. As a consequence of compressive deformation, the entire

Table 2. Stratigraphic subdivisions of some of the Neoproterozoic basins of India including present study (after Chaudhuri *et al.* 1999; Joy *et al.* 2019)

Group	Formation	Lithology	Facies
Vindhyan Basin			
Bhandar Group	Shikhoda Sandstone	Quartzose sandstone, mudstone	Intertidal shoal bar/barrier island
	Sirbu Shale	Mudstone, fine-grained sandstone	Lagoon-tidal flat
	Bundi Hill Sandstone	Quartzose sandstone	Beach-shoal bar
	Lakheri Limestone	Lime mudstone, stromatolitic limestone	Open carbonate ramp
	Ganurgarh Shale	Shale, mudstone	Lagoonal-tidal flat
Rewa Group	Govindgarh Sandstone	Pebbly and coarse sandstone	Fluvial
	Drammondganj Sandstone	Quartzose sandstone	Intertidal shoal bar
	Jhiri Shale	Shale, siltstone, sandstone	Deep prodelta
	Asan Sandstone	Pebbly sandstone and sandstone	Fan delta
	Panna Shale	Shale	
Cuddapah Basin			
Kurnool Group	Nandyal Shale	Calcareous shale	Subtidal
	Kolikuntala Limestone Paniam Quartzite	Limemuds tone, conglomerate quartzite and shale	Deep-water carbonate platform, shallow marine
	Nandyal Shale	Calcareous shale	Subtidal
	Paraconformity		
	Owk Shale	Shale with thin sandy interbeds	Subtidal
	Narji Limestone	Well-bedded lime mudstone	Deep-water carbonate platform
	Daiiganapalli Formation	Diamond-bearing conglomerate, sandstone, shale	Fan-delta (?)
Bhima Basin			
	Katageri Formation	Quartz arenite, shale, limestone	Tidal shelf
	Kerur Formation	Conglomerate, red-brown sandstone and shale	Fluvial to tidal
Pranhita-Godivari Valley			
Sullavai Group	Venkatpur Sandstone	Fine-grained subarkosic sandstone	Erg deposit
	Manclieral Quartzite	Ferruginous quartzose sandstone	Fan, braided fluvial
	Ramgiri Formation	Pebbly arkose, arkosic sandstone	
Shillong Basin			
Shillong Group	Umlapher Formation	Quartz mica schist	Deep-water siliciclastic
	Ingsaw Formation	Quartzite, micaceous quartzite	Shallow marine
	Tarso Formation	Polymictic conglomerate, gritty quartzite	Fan delta/alluvial fan

sediment package repeats on either side of the basal metaconglomerate (Fig. 2c, d). The polymictic metaconglomerate was therefore used as the marker horizon to regionally compare the stratigraphy, which indicates excellent regional control (see online Supplementary Fig. S2). It is worth noting in this section that Chaudhuri *et al.* (1999) considered a bottom non-repetitive polymictic conglomerate marker for interbasinal connections of India's Neoproterozoic basins (Table 2). Based on the observations of published articles and the current study, a basal polymictic conglomerate horizon is proposed for correlating unreported (if any) lowermost Neoproterozoic strata of India.

The detailed mapping, petrography, structural analysis and regional correlation during the present study conclude a very simple stratigraphy of Shillong Group, with three formations. For the lower, middle and upper formations, we propose the names 'Tarso', 'Ingsaw' and 'Umlapher', respectively. Tarso Formation

comprises a mixture of thick polymictic conglomerate and gritty quartzite. The major-oxide and trace-element geochemistry of the conglomerate samples indicates a mixed volcano-sedimentary source (sedimentary along with felsic volcanics) (Fig. 5a). However, the current study has limited scope for exploring the volcanogenic characteristics of the Shillong Basin metasediments. The conglomerate is occasionally graded and spatially variable in clast and matrix composition. Moreover, a texturally and mineralogically immature conglomerate is the characteristic of the Tarso Formation. The Ingsaw Formation is dominated by a quartzite-micaceous quartzite intercalation. The top and bottom part of the Ingsaw Formation is dominated by hard quartzite, whereas micaceous quartzite prevails in the middle part. The lowermost part of the unit is herringbone and trough cross-stratified, but the lower middle part is planar cross-stratified. Micaceous quartzite from the middle of the unit preserves occasional primary

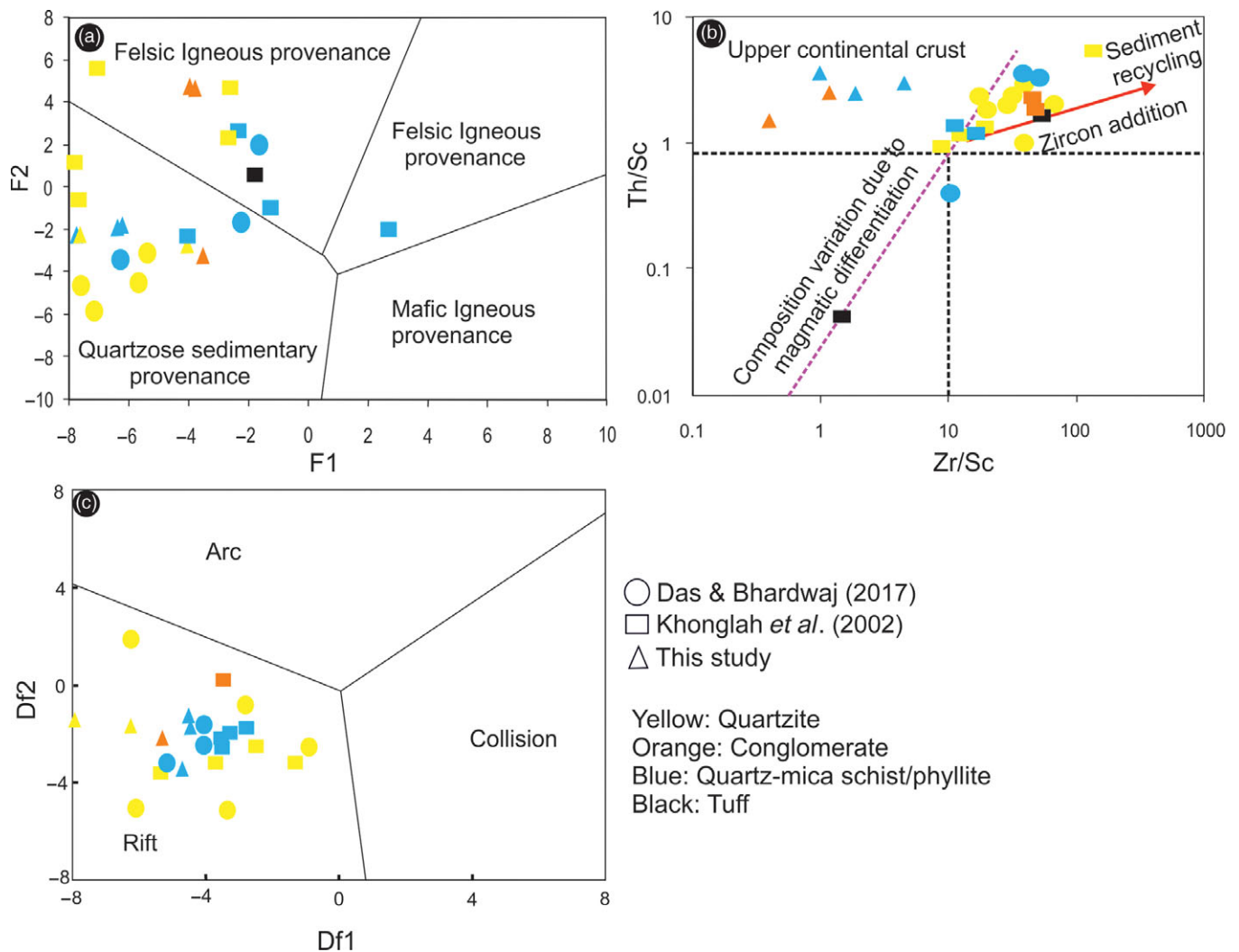


Fig. 5. (Colour online) (a) Discrimination diagrams for the origin of the sedimentary rocks of the Shillong Group using major oxides (after Roser & Korsch, 1988). $F1 = -1.773 \text{TiO}_2 + 0.607 \text{Al}_2\text{O}_3 + 0.76 \text{Fe}_2\text{O}_3(\text{total}) - 1.5 \text{MgO} + 0.616 \text{CaO} + 0.509 \text{Na}_2\text{O} - 1.224 \text{K}_2\text{O} + 9.09$; $F2 = 0.445 \text{TiO}_2 + 0.07 \text{Al}_2\text{O}_3 - 0.25 \text{Fe}_2\text{O}_3(\text{total}) - 1.142 \text{MgO} + 0.438 \text{CaO} + 1.475 \text{Na}_2\text{O} + 1.426 \text{K}_2\text{O} - 6.86$. (b) Shillong Group rocks plotted on a Th/Sr versus Zr/Sc bivariate diagram (after McLennan *et al.* 1993); average protolith compositions are of Proterozoic age (after Condie 1993). (c) Major oxide chemistry of all the representative samples of Shillong Group plots in rift setting in Df1 versus Df2 plot of Verma & Armstrong-Altrin (2013). $Df1 = 0.263 \ln(\text{TiO}_2/\text{SiO}_2) + 0.604 \ln(\text{Al}_2\text{O}_3/\text{SiO}_2) + 1.725 \ln(\text{Fe}_2\text{O}_3/\text{SiO}_2) + 0.66 \ln(\text{MnO}/\text{SiO}_2) + 2.191 \ln(\text{MgO}/\text{SiO}_2) + 0.144 \ln(\text{CaO}/\text{SiO}_2) + 1.304 \ln(\text{Na}_2\text{O}/\text{SiO}_2) + 0.054 \ln(\text{K}_2\text{O}/\text{SiO}_2) + 0.33 \ln(\text{P}_2\text{O}_5/\text{SiO}_2) + 1.588$; $Df2 = 1.196 \ln(\text{TiO}_2/\text{SiO}_2) + 1.064 \ln(\text{Al}_2\text{O}_3/\text{SiO}_2) + 0.303 \ln(\text{Fe}_2\text{O}_3/\text{SiO}_2) + 0.436 \ln(\text{MnO}/\text{SiO}_2) + 0.838 \ln(\text{MgO}/\text{SiO}_2) + 0.407 \ln(\text{CaO}/\text{SiO}_2) + 1.021 \ln(\text{Na}_2\text{O}/\text{SiO}_2) - 1.706 \ln(\text{K}_2\text{O}/\text{SiO}_2) - 0.126 \ln(\text{P}_2\text{O}_5/\text{SiO}_2) - 1.068$. Data source: Das & Bhardwaj (2017) and Khonglah *et al.* (2002).

structures. The upper quartzite is cross-stratified. The uppermost Umlapher Formation consists of quartz mica schist (Fig. 6). It is very thinly bedded and devoid of internal structures. The occurrence of felsic volcanics (tuff breccia, lapilli tuff, tuff and ignimbrite of rhyolitic to dacitic composition) in the upper Shillong Group has already been reported by Naik *et al.* (2020) from several sections of the Shillong Basin. The lowermost Tarso Formation of our study is partly correlatable with the Mawlyndep Formation, while the Umlapher Formation is comparable to the Umiam Formation of Khonglah *et al.* (2008).

In our observation, the Umsning Schist Belt of Khonglah *et al.* (2008) does not exist; instead, it is part of the Shillong Group repeating after the metaconglomerate due to folding (see online Supplementary Fig. S2). The metaconglomerate rests directly over the basement gneisses in the southwestern border, whereas quartzite lies directly over the basement 1 km away (Haokip *et al.* 2016). The basement cover relationship is therefore exposed either at the

margin of the deformed basin or deeply eroded places (see online Supplementary Fig. S2).

5.b. Depositional environment

Deposition of the Tarso Formation started with a texturally and mineralogically immature matrix-supported polymictic conglomerate. The matrix is micaceous at places (altered feldspar), and siliceous in others. The unfolding of the conglomerate gives an idea of lateral and vertical facies variation. The composition of the clasts varies along the strike length, depending on the variation in the protolith along the long axis of the rifted basin. The trace-element chemistry (Zr/Sc versus Th/Sc) of most of the samples suggests that Shillong Group sediments are recycled multiply from the provenance (Fig. 5b). Very poorly sorted angular clasts of the conglomerate indicate very short transportation and deposition in a sudden slope break (Fig. 7). It is quite similar to the modern slope wash/

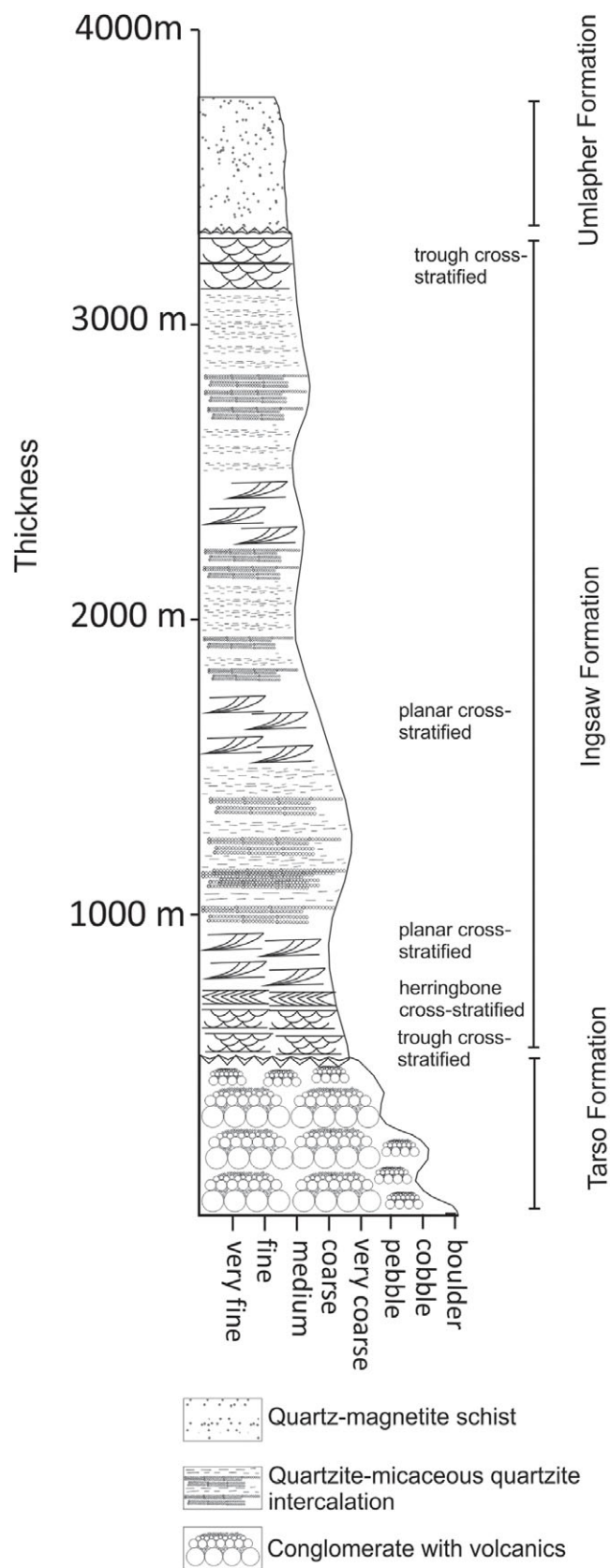


Fig. 6. Lithostratigraphy of Shillong Group of metasediments.

alluvial fan deposit. A comparable alluvial fan deposit characterizes the lowermost section of the Neoproterozoic Vindhyan, Cuddapah, Pranhita–Godavari, Marwar, Bhima and Kaladgi sub-basins of India (Table 2) (Chaudhuri *et al.* 1999; Patranabis-Deb *et al.* 2008; Saha & Patranabis-Deb, 2014; Joy *et al.* 2019). Most likely deposition of the Shillong Basin began with continental rifting. This is further substantiated by the major oxide chemistry of the metasediments, where the entire samples plot in the rift settings in the tectonic discrimination diagram (Fig. 5c) of Verma & Armstrong-Altrin (2013).

The sequence of graded bedding across the strike is indicative of either seasonal supply of sediments or fluctuation of flow strength. Naik *et al.* (2020) reported the existence of felsic volcanic rocks in the Shillong Group at various stratigraphic levels. However, the current study is not particularly focused on this aspect, and more concrete evidence is concerned with future investigation. Major oxide chemistry of the conglomerate matrix also shows a mixed provenance of quartz sedimentary and felsic igneous rock (Fig. 5a); contribution from volcanic rocks during the initiation of rift is therefore possible. However, the major oxide chemistry supports sediment recycling (Fig. 5b), that is, re-deposition of the basement’s ortho and paragneisses. A comparable rift-controlled passive margin deposition is reported from the Neoproterozoic basins of East Gondwana (Powell *et al.* 1994; Chaudhuri *et al.* 1999; Tack *et al.* 2001; Wang & Li, 2003; Jing *et al.* 2020; Lloyd *et al.* 2020). In the Neoproterozoic Officer Basin, the Savory Basin, the Adelaide Basin of Australia and the Nanhua Basin of China, the conglomerate is known to be a tillite deposit (Walter *et al.* 1995; Zhou *et al.* 2009; Lloyd *et al.* 2020). Despite the fact that the proposed continents were near to each other throughout the period under consideration, Chaudhuri *et al.* (1999) observed that glacial deposits from the lowermost section of India’s Neoproterozoic basins had not been documented. As a result, a more in-depth investigation in this area is required to explain why tillite deposits have not been found in the majority of India’s Neoproterozoic basins.

The conglomerate is followed by a discrete thin layer of trough cross-bedded quartzite and herringbone cross-stratified quartzite of the Ingsaw Formation. In the present context, the association of trough and herringbone cross-bedding above the conglomerate indicate a transitional marine condition where the initial fluvial state was interrupted by a tidal flat deposit of marginal sea (Fig. 7). Encroachment of the sea is apparent by the presence of herringbone structure, and the occurrence also marks a marine transgression at that period. The post-glaciation marine transgression during that span is recorded in all Neoproterozoic basins in East Gondwana (Walter *et al.* 1995; Zhou *et al.* 2009; Lloyd *et al.* 2020). Hence, sagging of the basin followed by sediment load finally caused entrance of seawater in a narrow linear basin. It was therefore an epeiric sea, partially enclosed within the continent. The fluctuation of current strength and direction in the tide-dominated delta in the lower part of the formation is evident from bipolar current movements and reactivation surface of herringbone cross-stratification. However, due to complex deformation, the preserved palaeocurrent direction is of little use in this study, although it can be used after cautious unfolding. The tidal sand ridges are noticeable from coarsening facies that pass from heterolithic beds upwards into planar/tabular cross-bedded sandstone. Herringbone cross-stratification is also restricted to certain places,

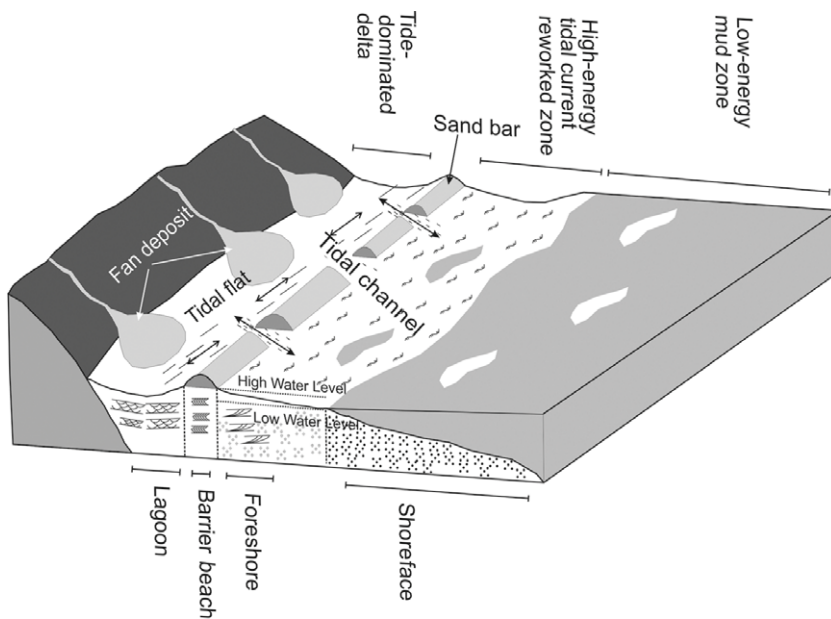


Fig. 7. Depositional environment for the Shillong Group of metasediments.

which indicates occasional dissection of sand ridges by tidal channels recording the bipolar current (Fig. 7). The presence of mud drapes (micaceous layers) is also indicative of tide-dominated shore. The middle and upper part of the quartzite is micaceous and, in places, thick layers of micaceous quartzite are preserved that probably indicate water-level fluctuation. Periodic water-level fluctuation is one of the common characteristics of Indian Neoproterozoic basins (Kale & Phansalkar, 1991; Chaudhuri *et al.* 1999). The presence of a significant amount of feldspars within the quartzite can be explained by the following factors: (1) cold climate; (2) physical disintegration exceeding chemical decomposition in the provenance; (3) rapid suspension-dominated transportation after disaggregation from the provenance bedrock and quick deposition; and (4) the proximal distance of the source. The rivers from the high altitude of the rifted basin might have contributed a considerable amount of deposit at high speed to the shelf. Again, the uppermost part of the formation is trough cross-stratified and coarse grained, indicating a drop in water level possibly caused by regression. The majority of India's Neoproterozoic basins show indications of a transgression in the early stage, followed by a regression (Chaudhuri *et al.* 1999).

The top Umlapher Formation is composed of micaceous quartzite, where the proportion of quartz is < 50% and indicates a low supply rate of clastic sediments. The secondary muscovites are a metamorphosed product of mud. In the present sedimentary environment, such facies are expected from distant shores where the supply of clastics is restricted. The Th/Sc ratio of the samples ranges from 2.5 to 3.5, implying an input from a felsic igneous component. When the current study is combined with the report of Naik *et al.* (2020) on the presence of felsic volcanics (metatuff of rhyolitic to dacitic composition) in the upper Shillong Group, it is possible to infer the significance of volcanic falls during deposition. However, the scope of this study does not include a detailed investigation of Shillong Group volcanic rocks. Moreover, in both cases the starvation of clastic sediments indicates deposition in relatively deeper-water facies (Fig. 7).

The above lithology and depositional environment show a fining-upwards sequence and shallow-water deposition throughout, implying that at the mature stage of evolution, the rate of

subsidence was accompanied by the rate of deposition. Similarly, a thick terrestrial and shallow-marine sequence was deposited in a series of Neoproterozoic intracratonic rift basins of peninsular and extra-peninsular India (Table 2), South China (Nanhua Basin), Western and Southern Australia (Adelaide Basin), and Eastern Antarctica (Kale & Phansalkar, 1991; Walter *et al.* 1995; Chaudhuri *et al.* 1999; Zhou *et al.* 2009; Rainbird *et al.* 2012; Lloyd *et al.* 2020).

5.c. Structural evolution of Shillong Basin

Mitra (1998) discussed four phases of deformations in the Shillong Group of rocks, whereas Khonglah *et al.* (2008) and Mero *et al.* (2016) argued for five and three stages of deformation, respectively. The detailed mapping of Shillong Group rocks in this study indicates two stages of coaxial folding caused by NE–SW compressional deformation. A progressive deformation caused tightening of the early folds, transposition of the early fabrics and, finally, plunging overturned, regional chains of antiform and synform (F_2). Western limbs of the regional/mapped scale F_2 are overturned with moderately SE-dipping axial plane. The Shillong Group metasedimentary rocks are thrust over the basement (AMGC) and the deformation patterns of both units are entirely different (except in the basin margin). The dominant fabric of the Shillong Group is NE–SW, but E–W for AMGC (Lal *et al.* 1978; Mitra, 1998; Chatterjee *et al.* 2007; Khonglah *et al.* 2008; Devi & Sarma, 2010; Ray *et al.* 2013). The possible oblique compression during basin closing has resulted in a NE–SW-aligned fold–thrust belt and steep shear zones (transpression) with down-plunging stretching lineations. The NE–SW sub-parallel transpression zones are themselves a small-scale replica of the collisional suture.

5.d. Geodynamic settings

Initiation of the basin is itself controversial (Mitra & Mitra, 2001; Bidyananda & Deomurari, 2007; Yin *et al.* 2010). Mitra & Mitra (2001) suggested that the early sedimentation of the Shillong Group started before 1550 Ma, based on the Pb–Pb age of syn-sedimentary galena. However, based on the report of the 900-Ma-aged population from the detrital zircons of the Shillong Group, Yin

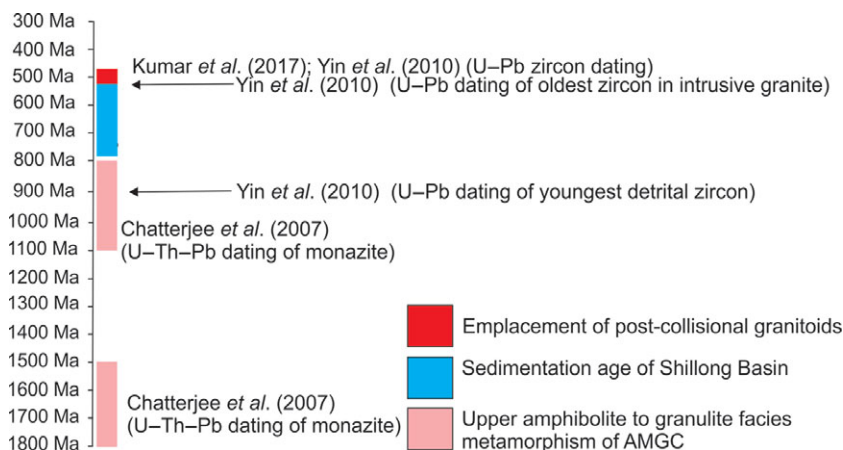


Fig. 8. (Colour online) Chronological evolution of Shillong Basin.

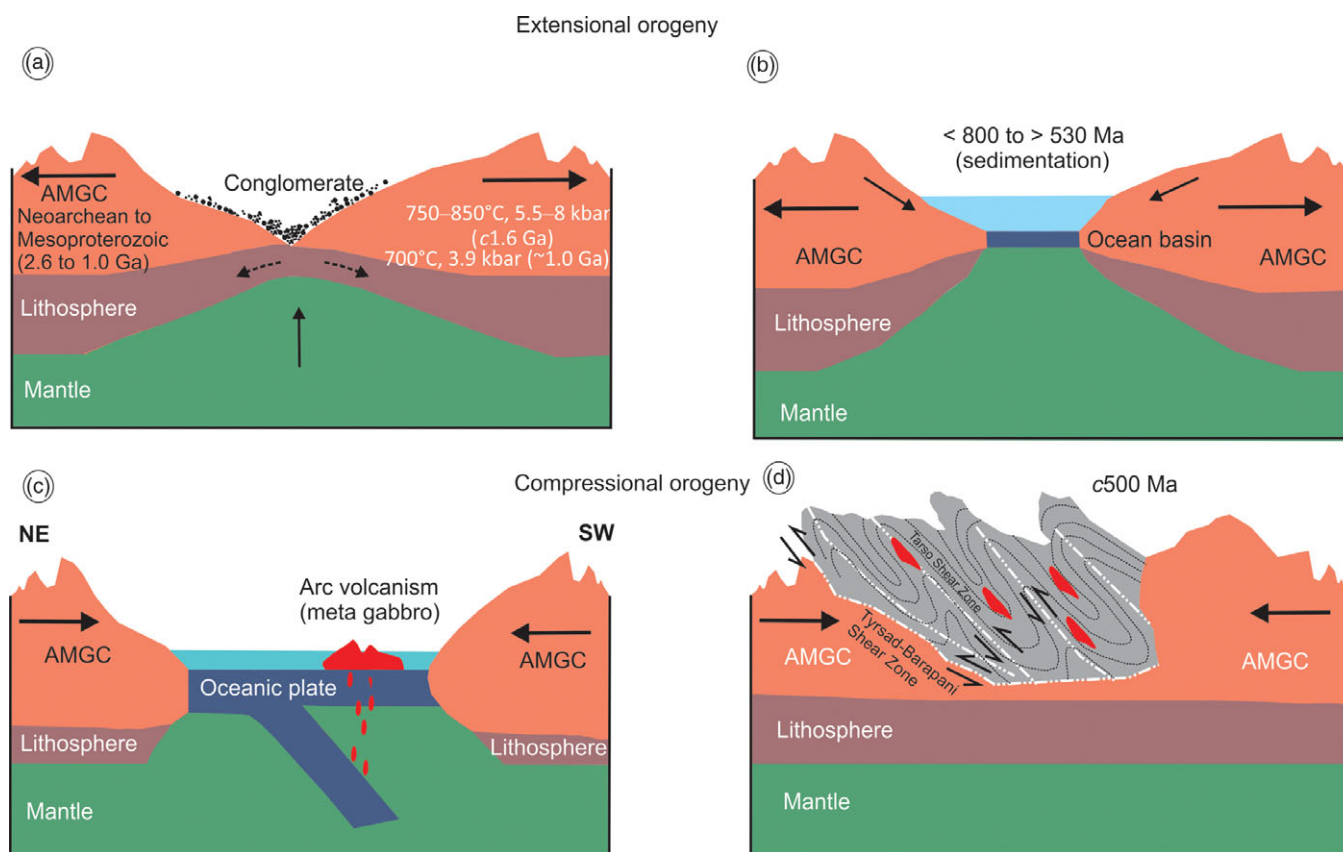


Fig. 9. (Colour online) Stepwise evolution of the Shillong Basin. (a) The basin was formed by rifting induced by lithospheric thinning caused by crustal extension, which resulted in asthenosphere rise. Rifting soon resulted in slope wash conglomerate deposition over the long basin axis. (b) Basin sagging followed by deposition caused encroachment of the sea in a landlocked condition and the deposition of shallow clastic sediments. (c) Initial collision during basin closing caused subduction of oceanic plate and emplacement of mafic rocks. (d) Finally, the collisional orogeny resulted in a fold-thrust belt at the mature stage of the orogeny.

et al. (2010) concluded that deposition began after that. Many workers have carried out extensive studies on the metamorphic evolution and thermal events of the AMGC (Lal et al. 1978; Chatterjee et al. 2007; Yin et al. 2010; Kumar et al. 2017; Neogi et al. 2017), and all concluded that the AMGC underwent three significant metamorphic (chemical dating of Monazites) and igneous events (U–Pb zircon dating), namely, at 1800–1500, 1100–800

and 500–450 Ma. The grade of metamorphism for the first two events (1800–1500 and 1100–800 Ma) was upper amphibolite to lower granulite facies (Lal et al. 1978; Chatterjee et al. 2007; Neogi & Pal, 2021) (Fig. 8). The Shillong Group, on the other hand, only witnessed greenschist metamorphism. High-grade metamorphism and accompanying deformations would be expected if deposited before 800 Ma. However, sedimentation before

800 Ma tends to be countered by the absence of basement deformation fabrics and high-grade metamorphism in the Shillong Group. The compiled geochronological data therefore indicate that deposition within the Shillong Basin commenced after c. 800 Ma (Fig. 8).

According to 900 Ma palaeomagnetic evidence from India, the Shillong Basin was quite close to Australia, Antarctica and South China during the Rodinia amalgamation (Cawood *et al.* 2013; Pant & Dasgupta, 2017) (Fig. 1a), and was very close to the orogenic front between the continents indicated. As a result, we believe that the intracontinental rifting (by possible underplating of magma or asthenospheric rise) in this section (the opening of the Shillong Basin) began during the Rodinia break-up (> 900 Ma) between Australia, South China and India. However, the current study does not report the concrete evidence of mafic magmatism from the lower section of Shillong Group rocks, which needs to be investigated further. However, the proposed impacts (plume-driven rifting) have been recorded across the entire belt, including the Adelaide Basin of Southern Australia, the Officer and Savory basins of Western Australia, the Beardmore Group of East Antarctica, Nanhua Basin of South China and Chungcheong Basin of South Korea (Walter *et al.* 1995; Goodge *et al.* 2002; Zhou *et al.* 2009; Bose *et al.* 2020; Kim *et al.* 2020; Kumar *et al.* 2020; Lloyd *et al.* 2020). As a result, in this study we assume that passive rifting via extension and the resulting asthenospheric rise is a plausible mechanism for the opening of the Shillong Basin (Fig. 9).

The upper age of the Shillong Basin is fixed (535–480 Ma) from U–Pb zircon dating of intrusive Cambrian granitoids (Yin *et al.* 2010; Kumar *et al.* 2017). So the entire episode of basin initiation, deposition, closing and associated deformation–metamorphism must have completed by that time (during 800–530 Ma) (Fig. 9). The closing of the Shillong Basin was responsible for the deformation as well as the metamorphism of the sedimentary rocks. It triggered the northwestern thrust of the sedimentary rocks over the basement with a tectonic contact, folding and low-grade metamorphism. The closing must therefore have initiated during the Gondwana amalgamation with initial subduction of the bottom oceanic crust, followed by late thrusting and folding of sedimentary rocks (Fig. 9). However, no obducted oceanic crust has been reported from the area so far, necessitating more research. Surprisingly, no comparable oceanic suture has been found throughout East Gondwana's collision belts (Powell & Pisarevsky, 2002). Due to the lack of subduction-related magmatism, Powell & Pisarevsky (2002) proposed an oblique sinistral transcurrent collision between India and Australia during the amalgamation of Gondwana. Sedimentation ended with the Pan-African Orogeny and widespread granite emplacement in all Neoproterozoic basins of India, Australia, Antarctica and South China (Goodge *et al.* 2002; Ghosh *et al.* 2005; Rainbird *et al.* 2012; Cawood *et al.* 2013; Valdiya, 2016; Kumar *et al.* 2017). As a result, the interval between the opening and closing of the Shillong Basin was calculated to be no more than 300 Ma.

An extensive field study, petrography, geochemistry, deformation fabric analysis and comparative study with other Eastern Gondwana Neoproterozoic basins suggest the continuity of the Gondwana Suture within the linear Shillong Basin, and we propose extending the Pan-African suture from the Eastern Ghat Mobile Belt (EGMB) in the south to the Shillong Basin in the NE (Fig. 1b).

6. Conclusion

- (1) The Shillong Basin, located in NE India, is an isolated Neoproterozoic basin with deformed and low-grade metamorphosed siliciclastic rocks.
- (2) The Shillong Group rocks are classified in the current study as lower Tarso Formation (conglomerate, gritty quartzite sequence), middle Ingsaw Formation (quartzite–micaceous quartzite sequence) and upper Umplapher Formation (magnetite-bearing quartz mica sequence).
- (3) The deposition of the Shillong Basin began with a polymictic conglomerate that was accompanied by shallow-marine sediments. The geochemistry of the metasediments indicates a rift-related setting for the deposits.
- (4) A preliminary stream-fed fan deposit converted to shallow-marine tidal flat and shelf deposit with multiple water-level fluctuations.
- (5) The integration of available geochronological data with field geology, petrography and geochemistry indicates that the Shillong Basin was opened up by rifting during Rodinia break-up (> 800 Ma, separation of India from Australia and South China), resulting in an epic sea condition.
- (6) The evolutionary history of the Shillong Basin is comparable to that of reported Neoproterozoic basins in peninsular and extra-peninsular India, Western Australia, Antarctica and South China (east Gondwana), all of which are rifting in origin and record shallow-marine clastic and/or non-clastic deposits (Walter *et al.* 1995; Chaudhuri *et al.* 1999; Goodge *et al.* 2002; Zhou *et al.* 2009; Joy *et al.* 2019; Bose *et al.* 2020; Kim *et al.* 2020; Kumar *et al.* 2020; Lloyd *et al.* 2020).
- (7) Basin closure was associated with the Pan-African collisional orogeny during Gondwana amalgamation, and the orogeny finally culminated with the intrusion of post-orogenic granitoids.

Supplementary material. To view supplementary material for this article, please visit <https://doi.org/10.1017/S0016756821001230>

Acknowledgements. The authors would like to thank the Director General of the Geological Survey of India and the Additional Director General of the Northeastern Region for their administrative assistance. Part of the work was completed during the GSI Field Season Program during 2017–2018. Michiel de Kock and Sojen Joy provided helpful feedback on the manuscript. We would also like to thank Olivier Lacombe for his efficient handling of the manuscript, and Sri Badu and Maiban for their assistance during fieldwork.

Declaration of interest. None.

Reference

- Ahmed M (1981) Stratigraphic classification of the Shillong Group, Khasi Hills, Meghalaya. *Journal of Mines, Metals and Fuels* 9, 295–7.
- Anonymous (2009) *Geology and Mineral Resources of Meghalaya*, first edition. Kolkata: Geological Survey of India.
- Arora D, Pant N, Pandey M, Chattopadhyay A, Greenbaum J, Siebert M and Bhandari A (2020) Insights into geological evolution of Princess Elizabeth Land, East Antarctica: clues for continental suturing and breakup since Rodinian time. *Gondwana Research* 84, 260–83.
- Barooah BC and Goswami ID (1972) Precambrian stratigraphy of the Assam Plateau. *Journal of Mines, Metal and Fuel* 20, 368–73.
- Bhattacharjee CC and Rahman S (1985) Structure and lithostratigraphy of the Shillong Group of rocks of East Khasi Hills of Meghalaya. *Bulletin Geological, Mining and Metallurgical Society of India* 53, 90–9.
- Bhowmik SK (2019) The current status of orogenesis in the Central Indian Tectonic Zone: A view from its Southern Margin. *Geological Journal* 54, 2912–34. <https://doi.org/10.1002/gj.3456>

- Bidyananda M and Deomurari MP** (2007) Geochronological constraints on the evolution of Meghalaya massif, northeastern India: an ion microprobe study. *Current Science* 93, 1620–3.
- Bilham R and England P** (2001) Plateau pop-up in the great 1897 Assam Earthquake. *Nature* 410, 806–9.
- Borah P, Hazarika P, Mazumdar AC and Rabha M** (2019) Monazite and xenotime U–Th–Pb total ages from basement rocks of the (central) Shillong–Meghalaya Gneissic Complex, Northeast India. *Journal of Earth System Science* 128, 68. <https://doi.org/10.1007/s12040-019-1085-x>
- Bose S, Banerjee DM, Jain AK, Dasgupta S and Bajpai S** (2020) Geology of the Proterozoic Eastern Ghats Belt: recent developments and outstanding issues. In *Special Issue of the Proceedings of the Indian National Science Academy: 36th IGC 2020 Geoscience Research in India*. The Indian Report to IUGS 2016–2020, 86, 87–97.
- Bradley DC** (2011) Secular trends in the geologic record and the supercontinent cycle. *Earth-Science Reviews* 108, 16–33.
- Cawood PA, Wang Y, Xu Y and Zhao Gd** (2013) Locating South China in Rodinia and Gondwana: a fragment of greater India lithosphere? *Geology* 41, 903–6.
- Chakraborty PP, Tandon SK, Roy SB, Saha S and Paul PP** (2020) Proterozoic sedimentary basins of India. In *Geodynamics of the Indian Plate*, pp. 145–177. Cham: Springer.
- Chatterjee N, Mazumdar AC, Bhattacharya A and Saikia RR** (2007) Mesoproterozoic granulites of the Shillong–Meghalaya Plateau: Evidence of westward continuation of the Prydz Bay Pan-African suture into Northeastern India. *Precambrian Research* 152, 1–26. <https://doi.org/10.1016/j.precamres.2006.08.011>
- Chaudhuri AK, Mukhopadhyay J, Deb SP and Chanda SK** (1999) The Neoproterozoic cratonic successions of peninsular India. *Gondwana Research* 2, 213–25. [https://doi.org/10.1016/S1342-937X\(05\)70146-5](https://doi.org/10.1016/S1342-937X(05)70146-5)
- Collins AS and Pisarevsky SA** (2005) Amalgamating eastern Gondwana: the evolution of the Circum-Indian Orogens. *Earth-Science Reviews* 71, 229–70.
- Condie KC** (1993) Chemical composition and evolution of the upper continental crust: contrasting results from surface samples and shales. *Chemical Geology* 104, 1–37.
- Das S and Bhardwaj A** (2017) Report on specialized thematic mapping for characterisation of Shillong Group of rocks and cover sediments, around Pynursla and Jarain, East Khasi Hills–Jaintia Hills districts, Meghalaya. Published Report. Kolkata: Geological Survey of India, 153 p.
- Devi NR and Sarma KP** (2010) Strain analysis and stratigraphic status of Nongkhyia, Sumer and Mawmaram conglomerates of Shillong basin, Meghalaya, India. *Journal of Earth System Science* 119, 161–74.
- George BG and Ray JS** (2017) Provenance of sediments in the Marwar Supergroup, Rajasthan, India: Implications for basin evolution and Neoproterozoic global events. *Journal of Asian Earth Sciences* 147, 254–70.
- Ghosh S, Fallick AE, Paul DK and Potts PJ** (2005) Geochemistry and origin of Neoproterozoic granitoids of Meghalaya, northeast India: Implications for linkage with amalgamation of Gondwana supercontinent. *Gondwana Research* 8, 421–32.
- Goodge JW, Myrow P, Williams IS and Bowring SA** (2002) Age and provenance of the Beardmore Group, Antarctica: constraints on Rodinia supercontinent breakup. *The Journal of Geology* 110, 393–406.
- Gregory LC, Meert JG, Bingen B, Pandit MK and Torsvik TH** (2009) Paleomagnetism and geochronology of the Malani Igneous Suite, Northwest India: implications for the configuration of Rodinia and the assembly of Gondwana. *Precambrian Research* 170(1–2), 13–26.
- Haokip L, Shijoh V, Srivastava A and Soraisam C** (2016) Report on Specialized thematic mapping of the Gneissic Complex, Shillong Group of rocks and Kyllang pluton between Nongtumai and Mairang areas, West Khasi Hill districts, Meghalaya. Published Report. Kolkata: Geological Survey of India.
- Jing X, Yang Z, Evans DA, Tong Y, Xu Y and Wang H** (2020) A pan-latitude Rodinia in the Tonian true polar wander frame. *Earth and Planetary Science Letters* 530, 115880.
- Joy S, Patranabis-Deb S, Saha D, Jelsma H, Maas R, Söderlund U and Krishnan U** (2019) Depositional history and provenance of cratonic “Purana” basins in southern India: A multipronged geochronology approach to the Proterozoic Kaladgi and Bhima basins. *Geological Journal* 54, 2957–79.
- Kakati P and Sarma KP** (2013) Porphyroblast–matrix relationships: a case study from metapelitic formation of Shillong Group, Meghalaya, India. *Indian Journal of Earth Science* 6, 1–13.
- Kale VS and Phansalkar VG** (1991) Purana basins of peninsular India: A review. *Basin Research* 3, 1–36. <https://doi.org/10.1111/j.1365-2117.1991.tb00133.x>
- Khonglah MA, Khan MA, Karim MA, Kumar A and Choudhury J** (2008) Geology and structure of the areas in and around Shillong, Meghalaya, North East India, revisited. *Nagaland University Research Journal* (ISSN 0973-0346), Special Publication, pp. 115–139.
- Khonglah MA, Khan MA and Kumar A** (2002) Report on specialized thematic mapping in parts of Barapani–Tyrasid Shear Zone, East Khasi Hills, West Khasi Hills and Ri Bhoi districts, Meghalaya, with special emphasis on the Basement and Shillong Group relationship. Published Report. Kolkata: Geological Survey of India.
- Kim SW, Kee WS, Santosh M, Cho DL, Hong PS, Ko K and Jang Y** (2020) Tracing the Precambrian tectonic history of East Asia from Neoproterozoic sedimentation and magmatism in the Korean Peninsula. *Earth-Science Reviews* 209, 103311.
- Kretz R** (1983) Symbols for rock-forming minerals. *American Mineralogist* 68, 277–9.
- Kröner A and Cordani U** (2003) African, southern Indian and South American cratons were not part of the Rodinia supercontinent: evidence from field relationships and geochronology. *Tectonophysics* 375, 325–52.
- Kumar N, Kumar N, Sharma R and Singh AK** (2020) Petrogenesis and tectonic significance of the Neoproterozoic magmatism of the Tusham Ring Complex (NW Indian Shield): insight into tectonic evolution of the Malani Igneous Suite and Rodinia Supercontinent. *Geotectonics* 54, 428–53.
- Kumar S, Rino V, Hayasaka Y, Kimura K, Raju S, Terada K and Pathak M** (2017) Contribution of Columbia and Gondwana Supercontinent assembly- and growth-related magmatism in the evolution of the Meghalaya Plateau and the Mikir Hills, Northeast India: Constraints from U–Pb SHRIMP zircon geochronology and geochemistry. *Lithos* 277, 356–75.
- Lal RK, Ackermann D, Seifert F and Haldar SK** (1978) Chemographic relationships in sapphirine-bearing rocks from Sonapahar, Assam, India. *Contributions to Mineralogy and Petrology* 67(2), 169–87.
- Li ZX, Bogdanova SV, Collins AS, Davidson A, De Waele B, Ernst RE and Karlstrom KE** (2008) Assembly, configuration, and breakup history of Rodinia: a synthesis. *Precambrian Research* 160, 179–210.
- Lloyd JC, Blades ML, Counts JW, Collins AS, Amos KJ, Wade BP and Drabsch M** (2020) Neoproterozoic geochronology and provenance of the Adelaide Superbasin. *Precambrian Research* 350, 105849.
- Mazumdar SK** (1976) *A Summary of the Precambrian Geology of the Khasi Hills, Meghalaya*. Kolkata: Geological Survey of India, Miscellaneous Publication 23, pt 2, pp. 311–334.
- Mazumdar SK** (1986) The Precambrian framework of part of the Khasi Hills Meghalaya. *Records of the Geological Survey of India* 117, 1–59.
- McLennan SM, Hemming SR, McDaniel DK and Hanson GN** (1993) Geochemical approaches to sedimentation, provenance, and tectonics. *Geological Society of America Special Paper* 284, 21–40. <https://doi.org/10.1130/SPE284-p21>
- Medlicott HB** (1869) Geological sketch of the Shillong Plateau in NE Bengal. *Memoirs of the Geological Survey of India* 7(1), 151–207.
- Mero A, Imlishila I, Sougrakpam S and Praveen S** (2016) Specialized thematic mapping of the Shillong Group, Myllem Granite around Laitkor, Myllem and Lingkardem area, East Khasi Hills District, Meghalaya. Published Report. Kolkata: Geological Survey of India.
- Mishra B** (2015) Precambrian metallic mineralization in India. In *Precambrian Basins of India: Stratigraphic and Tectonic Context* (eds R Mazumdar and PG Eriksson), pp. 327–37. Geological Society of London, Memoir no. 43.
- Mitra SK** (1998) Polydeformation of rocks of the Shillong Group around Sohiong, East Khasi Hills. *Indian Journal of Geology* 70, 123–31.
- Mitra SK and Mitra SC** (2001) Tectonic setting of the Precambrian of the northeastern India (Meghalaya Plateau) and age of the Shillong Group of rocks. *Geological Survey of India Miscellaneous Publication* 64, 653–58.
- Murthy MVN, Mazumdar SK and Bhaumik M** (1976) Significance of tectonic trends in the Geological evolution of the Meghalaya uplands since the

- Precambrian. *Geological Survey of India Miscellaneous Publication* **23**, 471–81.
- Nagarajan R, Madhavaraju J, Armstrong-Altrin JS and Nagendra R** (2011) Geochemistry of neoproterozoic limestones of the Shahabad formation, Bhima basin, Karnataka, southern India. *Geosciences Journal* **15**, 9–25.
- Naik RR, Theunuo K, Goswami TK, Khonglah MA, Pal T and Tripathy SK** (2020) Characteristics of Mesoproterozoic felsic meta-volcanics from the Shillong Group of rocks, Meghalaya, North East India. *Current Science* **118**(7), 00113891.
- Nandy DR** (2001) *Geodynamics of Northeastern India and the Adjoining Region*. Kolkata: ABC Publications.
- Neogi S, Kar S and Toshilila** (2017) Study on evolutionary history of high grade metamorphics of Sonpahar-Rambrai-Nongstoin area of West Khasi Hills District Meghalaya. Published Report. Kolkata: Geological Survey of India.
- Neogi S and Pal T** (2021) Metasomatically controlled sillimanite–corundum deposit: A case study from Sonapahar, Meghalaya, Northeast India. *Journal of Earth System Science* **130**, 1–15.
- Oldham T** (1858) On the geological structure of a portion of the Khasi, Bengal. *Memoirs of the Geological Survey of India* **1**(2), 270.
- Pant NC and Dasgupta S** (2017) An introduction to the crustal evolution of India and Antarctica: the supercontinent connection. In *Crustal Evolution of India and Antarctica: The Supercontinent Connection* (eds NC Pant and S Dasgupta), pp. 1–6. Geological Society of London, Special Publication no. 457.
- Patranabis-Deb S, Bickford ME, Hill B, Chaudhuri AK and Basu A** (2008) SHRIMP ages of zircon in the uppermost tuff in Chattisgarh Basin in Central India require ~500-Ma adjustment in Indian Proterozoic stratigraphy: A reply. *Journal of Geology* **116**, 540–2. <https://doi.org/10.1086/590127>
- Powell CM and Pisarevsky SA** (2002) Late Neoproterozoic assembly of east Gondwana. *Geology* **30**, 3–6.
- Powell CM, Preiss WV, Gatehouse CG, Krapez B and Li ZX** (1994) South Australian record of a Rodinian epicontinental basin and its mid-Neoproterozoic breakup (~ 700 Ma) to form the Palaeo-Pacific Ocean. *Tectonophysics* **237**, 113–40.
- Rainbird R, Cawood P, Gehrels G, Busby C and Azor A** (2012) The great Grenvillian sedimentation episode: Record of supercontinent Rodinia's assembly. In *Recent Advances in Tectonics of Sedimentary Basins* (eds C Busby and A Azor), pp. 583–601. Blackwell Publishing.
- Ray J, Saha A, Ganguly S, Balaram V, Krishna AK and Hazra S** (2011) Geochemistry and petrogenesis of Neoproterozoic Myliem Granitoid, Meghalaya Plateau, northeastern India. *Journal of Earth System Science* **120**(3), 459–73.
- Ray J, Saha A, Koeberl C, Thoni M, Ganguly S and Hazra S** (2013) Geochemistry and petrogenesis of Proterozoic mafic rocks from East Khasi Hills, Shillong Plateau, northeastern India. *Precambrian Research* **230**, 119–37.
- Rino S, Kon Y, Sato W, Maruyama S, Santosh M and Zhao D** (2008) The Grenvillian and Pan-African orogens: world's largest orogenies through geologic time, and their implications on the origin of superplume. *Gondwana Research* **14**, 51–72.
- Roser BP and Korsch RJ** (1988) Provenance signatures of sandstone-mudstone suites determined using discriminant function analysis of major-element data. *Chemical Geology* **67**, 119–39.
- Saha D and Patranabis-Deb S** (2014) Proterozoic evolution of eastern Dharwar and Bastar cratons, India - An overview of the intracratonic basins, craton margins and mobile belts. *Journal of Asian Earth Sciences* **91**, 230–51. <https://doi.org/10.1016/j.jseae.2013.09.020>
- Sarma KP** (2014) Shillong Supergroup: a New Lithostratigraphic Unit in the Basement – Cover Precambrian Rocks of the Shillong Plateau, Northeast India. *International Journal of Geology, Earth & Environmental Sciences* **4**(2), 158–71.
- Schöbel S, Sharma KK, Hörbrand T, Böhm T, Donhauser I and de Wall H** (2017) Continental rift-setting and evolution of Neoproterozoic Sindreth Basin in NW-India. *Journal of Earth System Science* **126**, 1–17.
- Tack L, Wingate MTD, Liégeois JP, Fernandez-Alonso M and Deblond A** (2001) Early Neoproterozoic magmatism (1000–910 Ma) of the Zadinian and Mayumbian Groups (Bas-Congo): onset of Rodinia rifting at the western edge of the Congo craton. *Precambrian Research* **110**, 277–306.
- Valdiya KS** (2016) Intracratonic Purana Basins in Peninsular India: Mesoproterozoic History. In *The Making of India* (ed. KS Valdiya), pp. 237–67. Switzerland: Springer, Society of Earth Scientists Series. https://doi.org/10.1007/978-3-319-25029-8_8
- Verma SP and Armstrong-Altrin JS** (2013) New multi-dimensional diagrams for tectonic discrimination of siliciclastic sediments and their application to Precambrian basins. *Chemical Geology* **355**, 117–33.
- Walter MR, Veevers JJ, Calver CR and Grey K** (1995) Neoproterozoic stratigraphy of the Centralian superbasin, Australia. *Precambrian Research* **73**, 173–95.
- Wang J and Li ZX** (2003) History of Neoproterozoic rift basins in South China: implications for Rodinia breakup. *Precambrian Research* **122**, 141–58.
- Yin A, Dubey CS, Webb AAG, Kelty TK, Grove M, Gehrels GE and Burgess WP** (2010) Geologic correlation of the Himalayan orogen and Indian craton: Part 1. Structural geology, U-Pb zircon geochronology, and tectonic evolution of the Shillong Plateau and its neighboring regions in NE India. *Geological Society of America Bulletin* **122**, 336–59.
- Zhou JC, Wang XL and Qiu JS** (2009) Geochronology of Neoproterozoic mafic rocks and sandstones from northeastern Guizhou, South China: coeval arc magmatism and sedimentation. *Precambrian Research* **170**, 27–42.